Galactic Abundance Gradients From IR Fine Structure Lines in Compact, H II Regions

A. Afflerbach & E. Churchwell
Department of Astronomy, 475 N. Charter St., University of Wisconsin, Madison, WI 53706

M.W. Werner
California institute of Technology, Jet Propulsion Laboratory, Pasadena, CA 91109

ABSTRACT

We present new observations of the [S III] 19pm, [0 111] 52 and 88μm, and [h' 111] 57pm lines toward 18 compact and ultracompact (UC) H 11 regions. These data were combined with data from the literature and high-resolution radio continuum maps to construct detailed statistical equilibrium and ionization equilibrium models of 34 compact H 11 regions located at galactocentric distances (D_G) O - 12 kpc. Our models simultaneously fit the observed IR fine-structure lines and hig}l-resolution radio continuum maps. Abundance gradients are found of the form [S / H] = (-4.45 ± 0.04) - (0.063 ± 0.006) D_G(kpc), [N / H] = (-3.58 ± 0.04) - (0.072 ± 0.006) D_G(kpc), and [0 / H] = (-2.85 ± 0.06) - (0.064 ± 0.009) D_G(kpc), and we derive T_e = (4560 ± 220) + (390 ± 40) D_G(kpc). The T_e gradient is consistent with the T_e gradient determined independently via radio recombination lines (Afflerbach *et al.* (1996). We observe no dependence of S / O, N / O, or T_{eff} *on* D_G. Gradients in N^{++} / 0^{++} and O^{++} / S^{++} are observed in the sense of increasing ionization with increasing DC;. This is entirely consistent with the decreased line blanketing with increasing D_G required by the above abundance gradients. All three gradients are best fit by a linear dependence on D_G. The abundances are consistent with production of sulfur, nitrogen, and oxygen by primary nucleosynthesis. Comparison with abundances in other galaxies implies a Hubble type between Sab and Sb for our galaxy and an unbarred or mixed galactic structure (Vila-Costas & Edmunds 1992). Our derived T_{eff} is 2000 K to 10000 K lower than T_{eff} expected from ZAMS stars of the same Lyman continuum flux (Panagia 1973; Vacca *et* al. 1996), probably due to uncertainties in the UV flux of stellar models for $E \geq$ 35. I eV, uncertainties in the luminosity-T_{eff} calibration, and/or ionization of H 11 regions by multiple stars in some sources.

1. INTRODUCTION

The distribution of galactic element abundances is a key to the chemical evolution of the galaxy. The present distribution of chemical abundances, or metallicities, in the galactic plane is a function of many variables: the historical star formation rate, the initial mass function, the relative yield of elements, homogeneity of the interstellar medium, infall of material from the halo, and radial inflows or outflows Of gas. Each of these processes may be functions of position and/or time. By determining the distribution] of metallicities in our galaxy, we should be able to provide important constraints on models of galactic evolution. Additionally, by comparing the distribution of galactic abundances to those in other galaxies, we can infer the morphology and other properties of our galaxy.

The form of the galactic abundance gradients is controversial. Shaver *et al.* (1983), Mezger *et* al. (1979), Churchwell & Walmsley (1975), and others find a decrease in metallicity with increasing galactocentric stellar evolution. Until now, UC H II regions have not been observed in surveys of galactic abundances. Because they appear to be more homogeneous than other candidate sources and are bright enough to be observed throughout the galaxy, they are a promising means of determining galactic abundances.

We selected sources for IR line observations based on the availability of high resolution radio continuum images, compactness, and excitation as high as permitted by source availability. Compact nebulae fit entirely within the KAO beam, so no correction for missing flux should be necessary. High excitation nebulae (ionized by a Lyman continuum photon flux greater than $10^{48.2}$) should have most O, N, and S in the doubly ionized state, so only small ionization corrections should be necessary to obtain atomic abundances.

Section 2 presents the FIR line and continuum observations and discusses data reduction; Section 3 presents detailed models of each source; Section 4 discusses derived properties of the nebulae; Section 5 discusses galactic abundances and compares the results to other models; and Section 6 summarizes the conclusions and recommends future work.

2. OBSERVATIONS

We selected a sample of UC H II regions to have 1) radio continuum fluxes $\geq$ 0.5 Jy to ensure that lines are observable; 2) high excitation (ionizing photon flux $\geq 10^{48.2}$ s^{-1}) so that the majority of the oxygen and nitrogen is probably doubly ionized; 3) compact nebulae, so that all the nebular flux is within the KAO beam; and 4) as wide a distribution as possible in galactocentric distance. To minimize confusion from nearby sources within the 45" beam of the KAO, it was preferable to observe spatially isolated sources, instead of UC H II *regions* in known clusters or complexes.

Observations were carried out on the nights of 9 and 13 June 1994 and the nights of 5, 9, and 11 August 1995 with the 91 cm telescope of the KAO using the facility Cryogenic Grating Spectrograph (CGS) developed by Erickson *et al.* (1984a, b, and 1985). Flights originated from the Ames Research Center at Moffett Field, CA in 1994 and Hickham Field in Honolulu, HI in 1995. The coordinates, observational parameters, and characteristics from the literature for each source are in Table 1. Guiding and boresight errors were ± 5". Sources were acquired from the offsets from stars in the HST Guide Star Catalog (Lasker *et al.* 1990; Jenkner *et al.* 1990). The chopper throw was 4'. Sequences of four integrations of ten seconds each were taken with the source placed alternately in the right and left beam.

For the [S III] 19 μm observations, an array of thirteen Ge:Be detectors was used. For the other wavelengths, we used an array of thirteen Ge:Sb detectors. The spectral resolution ($\lambda / \Delta\lambda$) for the 88, 57, 52, and 19 μm lines was 3920, 3505, 4470, and 4034, respectively. The profiles were unresolved by the spectrograph. A 5 mm aperture was used, providing FWHM aperture sizes of 36.4", 39.6", 40.1", and 43.2", respectively. Observations took place at altitudes from 35,000 to 41,000 feet, where observed lines are not strongly affected by telluric absorption. The H_2O vapor column was derived from observations of the 85.4 μm line toward Saturn; the H_2O vapor column ranged from 7 to 8 μm. Wavelength, atmospheric, and diffraction corrections have been applied to all spectra; each correction was typically <10%.

The absolute flux calibration was obtained by dividing each spectrum by a calibration spectrum of Saturn observed on the same flight. The expected emission of the disk of Saturn (Hanel *et* al. 1983; Bezard, Gautier & Marten 1986) was combined with the ring spectrum (Haas *et* al. 1982) using the technique of Matthews & Erickson (1977) to produce the calibration spectrum.

and 50000 K.

The input parameters for the models are the abundances of He, O, N, S, and Ne relative to hydrogen; T_{eff}, the temperature of the ionizing radiation field; N_c^*, the number of ionizing photons; $n_e(r)$, the electron density with position in the nebula; and f, the fraction of volume filled with gas. We iteratively determine the best-fitting parameters, constrained by our FIR line fluxes (Table 2) and radio continuum observations in the literature (Table 3).

From the continuum observations, we derive quantities useful for detailed modeling of the H II regions (Table 3). S_ν is determined from radio continuum images, generally of resolution $\sim 5''$ to ensure that we are observing flux on all spatial scales. S_ν is measured at a frequency where the emission is thought to be optically thin; for most H II regions, this is true for $\nu \geq 8$ GHz (Afflerbach *et al.* 1996; Kurtz *et* al. 1994; Wood & Churchwell 1989). We determine the Lyman continuum photon flux emitted by the star, N_c^*, from Rubin (1968) and Kurtz *et al.* (1994),

$$N_c^* = \frac{S_\nu}{(1.32\ 10^{-49})\xi a \nu^{-0.1} T_e^{0.5} D^{-2}}, \tag{1}$$

where S_ν^{SOURCE} is the total radio continuum flux in Jy (Table 3), ξ is the fraction of ionizing photons absorbed by gas, a is a constant approximately equal to one (Mezger & Henderson 1967), ν is the frequency of the radio continuum observation in GHz, T_e is the electron temperature of the H II region, and D is the distance from the Sun in kpc (Table 1). For our initial models, we assume $\xi = 1$, $a = 1$ and T_e = 8000 K.

We correct the IR line fluxes for extinction using the method of Simpson *et al. (1995). We* assume the extinction is proportional to the 9.7 μm optical depth in Table 3; for the ratio $\tau_\lambda/\tau_{9.7}$ we use 0.395 at 18.7 μm, 0.054 at 51.8 μm, 0.044 at 57.3 μm, and 0.019 at 88.4 μm (Simpson & Rubin 1990). All subsequent calculations and tables are corrected for extinction. For sources where we derive τ_λ directly from the 10 μm and 18 μm silicate features in the IRAS LRS spectra (Volk & Cohen 1989), we apply an approximation (Simpson 1994) based on the method of Simpson & Rubin (1990).

The core properties were determined from radio continuum images of spatial resolution ~ 1". These images are insensitive to flux on scale sizes > 10", therefore the spatial filtering of the large scale flux produces an image of the dense core component only. S_ν^{CORE} was determined from images of frequency $\geq$ 15 GHz, where the continuum is generally optically thin. θ_{proj} is the mean FWHM determined from the same images as S_ν^{CORE}. R_{sph} is the radius in arc-seconds of the core, determined from θ_{proj}, deconvolved from the beam, with the source modeled as a sphere (Mezger & Henderson 1967; Panagia & Walmsley 1978). We calculate from Mezger & Henderson (1967) an rms density $< n_e >$ such that a sphere of this density generates the observed S_ν^{CORE}. n_e is derived from $< n_e >$ assuming f = 0.1 (Afflerbach *et al.* 1994; Danks & Meaburn 1971) from the equation

$$n_e = \sqrt{\frac{< n_e^2 >}{f}} \tag{2}$$

(Osterbrock & Flather 1959).

3.2. One-Component Models

A summary of the modeling process is shown in Figure 1. We begin our iterations in Step 1 using N_c^* from Table 3. We assume f = 0.1. n_e in the region of IR line emission is estimated from the ratio of atmosphere that best reproduces the observed line fluxes; the error is dominated by the 40% uncertainty in O^{+} + / O; it is $\leq$ 1000 K for $T_{eff} \leq$ 35000 K, more for higher T_{eff} (Figure 2). The uncertainty is $\pm$ 26% in N / H and $\pm$ 28% in S / H, plus the measurement uncertainty in the relevant line ([N III] 57 μm or [S III] 19 μm) added in quadrature. The error is due to the uncertainties in the modeling process, including the uncertainty in S_{ν}, the ionization correction, N_c^*, the density distribution, the filling factor, T_{eff}, and extinction. Extinction can be as large as 2 magnitudes for the [S III] 19 μm line. The uncertainty in O / H is $\pm$ 45%, plus the measurement uncertainty added in quadrature. It is higher than the uncertainty for the S / H and N / H abundances due to the larger ionization correction factor for O / H. T_e is the mean temperature derived for the nebula; its uncertainty is $\pm$ 10%, due primarily to the uncertainty in O / H. Our analysis does not include possible errors in abundances due to the omission of dust, stellar winds, uncertainties in the stellar atmospheres, or uncertainties in atomic parameters.

Some sources in Table 1 could not be satisfactorily modeled. We were unable to fit a model to observations of G359.98+0.03 due to the poor quality of the radio continuum information. For G34.26, the geometry of the source (a dense cometary nebula and a separate, diffuse region with its own ionizing source) was incompatible with our spherically-symmetric, single-star models. G7.47, G12.21, and G11.95 were not observed in all the FIR lines necessary for a successful model. Abundances were derived for the sources G30.76, G30.78, and G291.61, and G291.63 from the data of Simpson *et* al. (1995) and presented in Table 4; however, T_{eff} for these sources is uncertain, because the source is not fully contained within the beam. Our models assume an ionization-bounded nebula fully contained within the beam; Simpson *et* al. (1995) find that this assumption may lead to an overestimate of T_{eff}.

4. DISCUSSION

4.1. Ionization

Because O^{+} and S^{+} have widely different ionization potentials, T_{eff} of the ionizing stellar atmosphere in our models is constrained by the observed ratio of the [O III] 52 μm line to the [S III] 19 μm line. Although we begin each detailed model by assuming the Kurucz (1991) stellar atmosphere T_{eff} corresponding to Lyman continuum photon flux (N_c^*) for ZAMS stars in Panagia (1973), our models indicate a much lower T_{eff} than the ZAMS models would assign to that Lyman flux (Figure 3). In this analysis we assume that the nebula is ionization bounded and that the gas absorbs all ionizing photons. If dust absorbs a significant fraction of ionizing photons, the discrepancies in Figure 3 between the models (Panagia 1973 and Vacca *et al.* 1995) and the observed fluxes would be greater. This is a well-known effect noted by several other groups, including Herter, Helfer & Pipher (1983).

We find an increase in T_{eff} with N_c^*, with a shallower slope than Vacca *et al.* (1996) and Panagia (1973) and an offset in T_{eff} ranging from 1000 to 2000 K at N_c^* = 48.2 to ~10000 K at N_c^* = 49.9. For 48 $\leq \log N_c^* \leq$ 49, the observed T_{eff} are consistent with model O stars of spectral class III. For 49.5 $\leq \log N_c^*$ <49.8, the observed T_{eff} are consistent with spectral class Ia (Vacca *et* al. 1996). Although we can be certain that compact H II regions are not ionized by evolved stars, the correlation of our derived T_{eff} with models of spectral class III and Ia may imply that the ionizing stars are more luminous than predicted by Panagia (1973) and Vacca *et al.* (1996).

Uncertainties in the stellar atmospheres in the UV may lead to a systematic uncertainty in T_{eff} in our models. The O^{++} / O ratio depends extremely sensitively on the distribution of photons with $E \geq$ 35.1 eV, the ionization potential of O^{+}. Massive stars are expected to have winds which produce significant.

drop as quickly with distance from the center as in the cooler stat. The region of doubly ionized oxygen coincides with the H II region.

The metal ions have a significant effect cm the nebular radiation field. The result of bound-free interactions with ions can be seen whine J_E increases slightly at each ionization edge. The increase is strongest for O^+ due to the high abundance of oxygen. Photoionization of ions is a significant source of opacity. The opacity is so large, that, in many cases, increasing the abundances in the models leads to a decrease in the [0 111] and [N 111] line fluxes, because the average ionization of the nebula has decreased. This effect has also been pointed out by Rubin (1983, 1985). In a two-component, core-halo model, the oxygen equilibrium is also affected by the size and ***density*** of the core, since the [O 111] IR line fluxes depend strongly on the extent of the O^{++} ionization zone into the diffuse halo component.

The feature between 19 and 22 eV in Figure 4 is due to the recombination line of helium from the 2^3S level. This line is highly forbidden and is considered by the code to be in the diffuse radiation field. The emission of the line was modeled to give the accurate emissivity of the line and the correct distribution of the energy released. This change in the modeling of the line for ease of computatoin does not affect the ionization equilibrium or statistical equilibrium.

We note that most of the spectra in Figure 4 do not show evidence of hardening because the opacity of neutral hydrogen is very low. Therefore the change in the radiation field with increasing radial distance is due primarily to geometric dilution.

Figure 5 shows the derived ionization correction factors as a function of T_{eff} of the ionizing star. We see satisfactory agreement with the theoretical ionization correction factors in Figu re 2. The ionization fraction O^{++} / O increases with T_{eff} with a large scatter due to differences in density structure and Lyman continuum photon ftux (A';) of the nebulae, The ratio N^{++} / h' > 0.7 in all but 5 cases (where $T_{eff} \lesssim$ 3400() K), and it generally stays near unity. The ratio S^{++} / S is also near unity, though there is evidence of an increasing fraction of S^{+3} for $T_{eff} \gtrsim$ 38500 K.

5. GALACTIC PROPERTIES

5.1. Abundances

From the derived N / H, S / H, and O / H in Table 4 we can obtain the distribution of abundances as a function of galactocentric distance D_G. The data arc displayed in Figures 6a, 6b, and 6c. Linear least squares fits to the data, displayed as solid lines, arc:

$$[N/n] = (-3.583\ 0.04) - (0.072A\ 0.006)\,D_G(\mathrm{kpc})\,(r = -0.76), \tag{3}$$

$$[S/H] = (--4.45*\ 0,04) -- (0.0633\ 0.006)\,D_G(\mathrm{kpc})\ (r= --0.77), \tag{4}$$

and

$$[O/H] = (-2.854\ 0.06) - (0.0644.\ 0.009)\ D_G(\mathrm{kpc})\ (r= -0.66), \tag{5}$$

where ***r*** is the correlation coefficient. Thus N / H, S / H, and O / H decrease with increasing D_G. A constant slope is statistically superior to a two-step distribution of abundances. We observe greater scatter in the abundances among sources with D_G > 6 kpc than those with D_G < 6 kpc. Due to the ionization correction, O / H has more scatter than N / H or S / H.

5.1.2. *The S / H Gradient*

We derive S / H abundances equivalent to those of Simpson *et al.* (1995) and Simpson & Rubin (1990). For the sources where we used line fluxes from Simpson *et al.* (1995), our derived S / H generally agree with those of Simpson *et al.* (1995) within the errors. Our gradient is also consistent with results of Maciel & Köppen (1993) for all types of planetary nebulae except those with low-mass progenitors, which are thought to be older than 6 Gyr. Shaver *et al.* (1983) did not find a S / H gradient with D_G from their data. However, there were only a few sources (14) for which they had sulfur line data, and for which the sulfur abundances were derived. An S / H gradient may not have been detected by Shaver *et al.* (1983) because of the weakness of the [S III] λ6312Å line, the small number of sources distributed over a small fraction of the galactic disk, and an uncertain ionization correction for sources which were only observed in [S II] lines.

5.1.3. *The O / H Gradient*

The O / H abundances we derive are consistent with the results found by Shaver *et al.* (1983) for diffuse H II regions and with those inferred by Afflerbach *et al.* (1996) for UC H II regions. Our gradient is consistent with the results of Maciel & Köppen (1994) for all types of planetary nebulae except for the youngest nebulae, which have a shallower slope and a large dispersion in O / H abundances. Our gradient is shallower than that found by Peimbert (1978), who observed a slope in [O / H] with D_G of -0.13 ± 0.04, for five H II regions in the range 6.5 - 11.8 kpc.

Our results are inconsistent with those of Kaufer *et al.* (1994), who find no dependence of O / H and N / H on D_G in the range 6.0- 17.0 kpc in B stars in the galactic plane. It may be significant that the abundances derived by Kaufer *et al.* (1994) appear to scatter by ~ ±0.3 dex around the mean value. If this scatter is in fact the result of uncertainties in the determination of individual abundances, it is possible that a gradient with the slope we observe could be hidden in the noise. This is especially true for D_G >6.0 kpc, where we observe somewhat more scatter in our abundances and possibly a shallower gradient than in the inner galaxy.

5.1.4. *Scatter of Abundances*

To distinguish the intrinsic scatter of the abundances at a given D_G from the random errors due to measurement uncertainties and model errors, we apply a procedure described by Savage et al. (1990). We estimate the intrinsic scatter in the abundances using a parameter σ_i added in quadrature to the uncertainties we determined for each point. If we adjust σ_i to make the reduced χ^2 equal to unity, we derive an intrinsic scatter σ_i = 0.16, 0.10, and 0.16 for log (N / H), log (S / H), and log (O / H), respectively. The agreement of σ_i for the three elements demonstrates the consistency of our modeling process and our derived errors. We infer a systematic intrinsic scatter of $\lesssim$25 - 45% in the abundances for a particular D_G. The intrinsic scatter of abundances may result from incomplete mixing of the ISM or non-radial variations in abundances due to spiral structure. However, we caution that some of this scatter may be due to unknown systematic errors in our modeling process due to the omission of dust and stellar winds, the assumption of a one or two-component density distribution, or uncertainty in the model stellar atmospheres or atomic coefficients.

determined from the same class of regions via radio recombination lines. The fact that the T_e-D_G gradient found from modeling our IR line observations is essentially the same as that found from modeling RRL line observations of the same class of nebulae provides strong support for the conclusion of Afflerbach *et al.* (1 996) that the T_e-D_G distribution is primarily determined by the distribution of the abundances of nebular coolants aud secondarily by the effects of collisional quenching of coolant lines. In addition, we find from our analysis that S / H, h' / H, and O / H have approximately the same gradients in the galactic plane from 0 - 11.4 kpc.

5.3. Abundances and ionization Gradients From Ion Ratios

By considering the ion ratios O^{++} / S^{++} and N^{++} / O^{++} and T_{eff} as a function of D_G, we can investigate the variation of ion abundance ratios with element abundance variations within the galaxy. Figures 8a and 8b show the N^{++} / O^{++} and O^{++} / S^{++} ratios as a function of D_G. Although there is substantial scatter due to variations in density structure and N_c^* among the sources, it is clear that O^{++} / S^{++} is greater at $D_G > 5$ kpc than at $D_G < 5$ kpc, and that N^{++} / O^{++} is lower at $D_G > 5$ kpc than at D_G <5 kpc. This correlation is in the sense of increasing ionization with increasing D_G, in agreement with FIR observations by Simpson *et al.* (1995) and He recombination line observations by Churchwell *et* al. (1976). However, the modeled T_{eff} dots not show an increase with D_G in our sample, as would be the case if the ionizing stars increased in excitation with D_G. We therefore conclude that the increased ionization with D_G is not due to a systematic increase in T_{eff} with D_G, but rather to the change in abundances with D_G, as discussed below.

In Figure 9a, our ionization equlibrium models show that O^{++} / S^{++} clearly increases with T_{eff}, but that there is also an additional effect which causes the ratio to increase with D_G, independent of T_{eff}. From models of H II regions over the observed range of abundances ([Z / H] = -0.4 Orion to 0.8 Orion), we see that this variation in O^{++} / S^{++} is expected from the observed range of metallicities, and that it is likely that the observed increase in ionization with D_G is due to a decrease in opacity due to decreased line blanketing (Searle 1971; Shields 1974). A fully sc]f-consistent treatment would include the same abundances in the model atmospheres as in the nebula. This is beyond the scope of this paper but should be done in future analyses. Including the change in line blanketing due to the change in abundances with D_G in the stellar atmosphere models would impact the inferred stellar effective temperature T_{eff}. A change in T_{eff} would have the strongest impact on the derived O / H but should have a significantly smaller effect on N / H and S / H.

When wc include the additional scatter in the theoretical determinations of log(O^{++} / S^{++}) of ± 45% due to the variation of n_e and N_c^* within our sample, We find that all but four sources have values of log(O^{++} / S^{++}) that fat] within the range of the models. G298.22 has a low O^{++} / S^{++} for its observed T_{eff} = 40000 K, because it is ionized by multiple sources, and also because the source is not fully contained within the beam, both resulting in an overestimate of T_{eff}.

A similar analysis applies for the ratio N^{++} / O^{++}. The decrease in the ratio with D_G, to a large extent, is due to an increase in ionization with D_G, which is consistent with the observed decrease in abundances with increasing D_G. In this case the scatter in D_G due to the range of n_e and N_c^* is ± 1570, much smaller than for O^{++} / S^{++}. All but four sources fall within the range of our models. our O^{++} / S^{++} and N^{++} / O^{++} gradients are consistent with the ionization gradient duc to decreasing metallicity with increasing D_G.

(1 ,ar son 1976; Matteucci & Francois 1989; and others) and / or a thick disk (Pardi *et al.* 1995) which takes place at galactocentric distances which increase linearly with time.

The distribution of relative abundances in the galactic plane is thought to be primarily due to the history of stellar nucleosynthesis. The production of an element in primary nucleosynthesis is independent of the initial composition of the stare that produce it and is likely to be the result of α-process nucleosynthesis (Vila-Costas & Edmunds 1993). In secondary nucleosynthesis, the yield of an element is a function of the initial abundance of seed elements. If the majority ^{14}N is produced via secondary nucleosynthesis in the CNO process, the ratio of N to primary elements can be expected to increase with the abundance of the primary elements (Vila-Costas & Edmunds 1993; Edmunds & Pagel 1978) and, therefore, decrease with increasing D_G.

We observe a gradient of N / H decreasing with increasing D_G which has the same slope as the gradient for the primary element sulfur. N /O is not found to be a strong function of D_G. The implication is that the majority of nitrogen is produced through primary nucleosynthesis. This production of nitrogen may take place in the third dredge-up from the CO core during the AGB phase (Renzini & Voli 1981; Iben & Renzini 1983) or in stars of low metallicity of mass > 30 $M_{\odot}$ (Woosley *et al.* 1993). Alternately, nitrogen may be produced mostly try secondary nucleosynthesis, but the h' / O gradient may have been flattened due to pollution of unprocessed material by supernovae in other regions o f the galaxy (Wilmes & Köppen 1995).

The observed decrease of S / H with D_G, along with the lack of a clear dependence of S / O on D_G is consistent with primary nucleosynthesis of S and O. This resolves the problem of the apparently flat distribution of S / H with D_G observed by Shaver *et* al. (1983) which could not be explained by nucleosynthesis models without postulating a difference in the timescale of S and O production] (Matteucci & Francois 1989; Matteucci 1991).

For S / H and N / H a single gradient with D_G is statistically more significant than a step function for D_G < 11.4 kpc, although the increased scatter of abundances at D_G > 6 kpc may allow for flattening of the gradient in the outer galaxy. Therefore we do not see evidence of the radial mixing in the inner galaxy that would be the result of a strongly barred structure (Friedli *et* al. 1994). The absence of a strongly-barred structure in our galaxy is also consistent with the magnitude of the abundance gradient and the absolute value of abundances in the galactic center (Section 5.4).

6. CONCLUSIONS

The main results of this work are as follows:

1) Observations of [0 111] 88 and 52 pm, [h' III] 57 μm, and [S 111] 19 pm IR fine-structure lines are reported for a sample of 34 compact and UC H II regions distributed in the galactic plane from O - 12 kpc.

2) Internally consistent statistical and ionization equilibrium nebular models with line blanketed Kurucz (1 991) atmospheres were produced for each source consistent with the observed IR fine-structure lines and high-resolution radio continuum images. Where appropriate, models included two density components.

3) We find abundances which decrease with increasing Dc. We derive the gradients: [S / H] = (-4.45 ± 0.04) - (0.063 ± 0.006) D_G (kpc), [N / H] = (-3.58 ± 0.04) - (0.072 ± 0.006) D_G (kpc), and [O / H] = (-2.85 ± 0.06) - (0.064 ± 0.009) D_G (kpc). All gradients have the same slope, and the abundances are trotter fit by a single gradient than by two components or by a step function of D_G. The intrinsic scatter of

Table 1: Observational Parameters

Source	α (1950)" hh mm ss.s	δ (1950) ° ′ ″	Date	D (kpc)	D_G (kpc)
G359.98-0.08 (Sgr "A A/B)	174241.5	-285822	5/93	8.5[f]	0.0[f]
G359.98+0.03 (Sgr A H2)	174218.0	-2854 55	5/93	8.5[f]	0.0[f]
G5.97-1.18 (M8)	180036.4	-242254	8/95	1.9[a]	6.6[a]
G7.47+0.06	175911.8	-222802	8/95	6.3[b]	2.4[b]
G8.14-0.23	180000.9	-214813	8/95	3.7[a]	4.9[a]
G9.61+0.20B	180315.3	-203204	8/95	5.7’	3.0’
G11.95-0.03	180856.2	-183658	8/95	4.4[d]	4.3[d]
G12.21-0.10	180943.7	-182509	8/95	13.4[a]	5.4’
G24.47+0.49	183126.7	-072024	6/94	9.4[b]	3.9[b]
G25.38-0.18	183533.6	-065034	6/94	10.8[b]	4.8[b]
G25.4-0.14	183526.8	-064838	6/94	9.6[b]	4.1[b]
G32.80+0.19	184756.8	-000535	6/94	13.0[b]	7.5[b]
G34.26+0.15	185046.2	011113	6/94	3.6’	5.9[a]
G37.87-0.40	185924.7	040826	6/94	9.2[a]	5.8[a]
G61.47+0.10 (s88 B)	194443.5	250522	6/94	2.0’	7.7[a]
G75.84+0.40	201947.3	372126	6/94	4.7[a]	8.7’
G81.7+0.5 (DR 21)	203714.1	420854	6/94	2.0’	8.6[a]
G105.63-O.34 (S138)	223052.6	58 12 48	6/94	6.3’	11.4’
G108.19+0.58 (S146)	224730.7	593856	6/94	5.2[e]	11.2’
G108.76-0.95 (S152)	225636.4	583046	6/94	5.3’	11.3[e]

[a] Kurtz 1996

[b] Garay *et al.* 1993

[c] Hofner *et al.* 1994

[d] Wink, Altenhoff, & Mezger 1982

[e] Rudolph 1994

[f] Galactic Center

Table 2: Observed Line & Continuum Fluxes (continued)

Source	Line Flux (10^{-18} W cm^{-2}) Continuum Flux (Jy) t_{ir} ,s)			
	[S III] 19μm	[O III] 52μm	[N III] 57μm	[O III] 88μm
G37.87	6.3±1.0 "-"	31.5±2.3	7.4±0.8	9.7±0.7
	69±44	1994±181	28373220	34353286
	240	240	240	600
G61.47	7.63.2.1	16.441.5	3.330.9	2.840.4
	381 ±96	59723429	5349±391	70713.510
	240	160	320	160
G75.84	65.0±4.9	115.8± 8.2	20.831.6	26.732.2
	386±75	40713339	3967± 333	38043.284
	160	360	280	160
G81.7	2.8* 1.6	12.541.1	6.931.0	4.130.4
	226±66	5440±421	7172±531	108914766
	240	160	280	400
G105.63	2.4±0.8	2.140.4	0.730.2	1.1±0.1
	72±43	779396	869370	889±68
	480	480	480	480
G108.20	21 .3*3.3	36.553.0	6.730.8	16.931.2
	2953157	8735169	6625106	647398
	80	80	120	160
G108.76	16.041.4	6.6±0.8		4.030.6
	1673.71	9015-129		693382
	80	240		160

Table 4: Results

Source	D_G (kpc)	n_e (cm^{-3})	T_{eff} (K)	O^{++}/O	S^{++}/S	N^{++}/N	S/H (10^{-5})	N/H (10^{-5})	O/H (10^{-5})	T_e (K)
G359.98	0.0	4000	32500	0.23	0.96	0.86	2.6	38.1	64	6300
G5.97	6.6	1400	33500	0.63	0.80	0.96	2.0	9.7	69	6700
G8.14	4.9	800	32500	0.21	0.96	0.80	1.3	7.6	59	720(1
G9.61B	3.0	650	31500	0.03	0.97	0.42	2.1	7.3	58	6300
G24.47	3.9	825	35000	0.12	0.96	0.74	2.3	13.6	100	6100
G25.38	4.8	1200	37500	0.28	0.94	0.85	1.6	16.3	85	6700
G25.4	4.1	120C	34000	0.06	0.97	0.49	1.5	9.8	84	6700
G32.80	7.5	250C	38750	0.77	0.74	0.96	1.2	7.3	18	10800
G37.87	5.8	hoc	38750	0.84	0.65	0.98	1.2	12.0	46	8700
G61.47	7.7	5750	32500	0.40	0.94	0.90	0.49	3.4	23	9800
G75.84	8.7	2100	36250	0.61	0.86	0.95	0.71	5.7	32	8800
G81.7	8.6	210G	31500	0.15	0.97	0.68	0.65	2.7	27	9300
G105.63	11.4	175	32500	0.45	0.92	0.91	0.34	3.0	16	11200
G108.2O	11.2	650	34500	0.53	0.89	0.94	0.64	3.7	31	8500
G108.76	11.3	400	32000	0.10	0.98	0.62	0.71		38	8400
G0.1	=To--	175	32500	0.03	0.97	0.33	3.0	[illegible]	210	4400
G1.13	0.2	800	34500	0.14	0.97	0.86	3.3	20.7	190	4700
G10.30	3.6	200	34000	0.34	0.93	0.91	3.3	19.0	110	5900
G10.32	3.6	800	33500	0.08	0.98	0.77	5.1	20.4	240	3900
G23.95	4.3	2200	32500	0.21	0.96	0.85	2.4	10.1	50	7300
G29.96	4.3	750	37500	0.60	0.83	0.96	2.2	18.2	56	7800
G30.76S[a]	4.7	600	35000	0.31	0.95	0.90	2.1	24.0	106	5500
G30.76C[a]	4.7	600	35000	0.35	0.94	0.92	2.3	23.9	104	5300
G30.78N[a]	4.7	775	35000	0.24	0.95	0.86	1.6	15.6	80	6500
G45.12	6.4	1700	36250	0.41	0.91	0.91	0.51	3.2	18	10500
G45.45	8.2	850	35000	0.28	0.93	0.88	1.5	6.8	82	6800
G49.49	6.7	1600	36250	0.54	0.88	0.94	1.1	10.2	50	7600
G70.3	9.9	750	38750	0.85	0.65	0.98	1.(I	5.9	20	10600
G110.1	10.2	650	32500	0.40	0.93	0.91	1.1	5.5	32	9000
G291.28	7.9	8000	3'8750	0.75	0.76	0.97	1.6	9.2	68	7400
G291.61[a]	8.9	900	38750	0.71	0.80	0.96	1.6	13.3	89	6100
G291.63[a]	8.9	950	38750	0.58	0.87	0.94	1.4	12.0	88	6400
G298.22	9.9	1900	40000	0.34	0.92	0.79	0.77	3.8	50	8600
G333.6	6.0	4000	34500	0.22	0.96	0.81	0.98	5.6	38	8600

[a] Full nebula not in beam

Hanel, R. A., Conrath, B. J., Kunde, V. G., Pearl, J. C., & Pirraglia, J. A. 1983, Icarus, 53, 262

Henry, R. B. C. & Howard, J. W. 1995, ApJ, 438, 170

Herter, T., Helfer, H. L., Pipher, J. L. 1983, A&AS, 51, 195

Hoare, M. G., Drew, J. E., & Denby, M. 1993, MNRAS, 262, L19

Hofner, P., Kurtz, S., Churchwell, E., Walmsley, C. h4., & Cesaroni, R. 1994, ApJ, 429, L85

Howard, J. W., Henry, R. B. C., & McCartney, S. 1996, ApJ, in prep

Iben, I., Jr. & Renzini, A. 1983, A&A Rev., 21, 271

Jenkner, H., Lasker, B. M., Sturch, C. R., Mc Lean, B. J., Shara, M. M., & Russell, J. L. 1990, AJ, 99, 2082

Kaufer, A., Szeifert, Th., Krenzin, R., Baschek, B., & Wolf, B. 1994, A&A, 289, 740

Kurtz, S. 1996, private communication

Kurtz, S. & Churchwell, E. 1996, ApJS, in prep

Kurtz, S., Churchwell, E., & Wood, D. O. S. 1994, ApJS, 91, 659

Kurucz, R. L. 1991, in IAU Symposium 149, Stellar Populations of Galaxies, ed. B. Barbuy & A. Renzini (Dordrecht: Reidel), 225

Larson, R. B. 1976, MNRAS, 176, 31

Lasker, B. M, Sturch, C. R., Mc Lean, B. J., Russell, J. L., Jenkner, H., & Shara, M. M. 1990, AJ, 99, 2019

Lester, D. F., Dinerstein, H. L., Werner, M. W., Watson, D. M., Genzel, R., & Storey, J. W. V. 1987, ApJ, 320, 573

Maciel, W. J. & Köppen, J. 1994, A&A, 282, 436

Mathis, J. S. 1985, ApJ, 291, 247

Matteucci, F. & Francois, P. 1989, MNRAS, 239, 885

Matteucci, F. 1991, in Frontiers of Stellar Evolution, ed. D. L. Lambert (San Francisco: ASP), 539

Matthews, S., & Erickson, E. F. 1977, NASA TM, X-73, 204

Mehringer, D. M., Palmer, P., Goss, W. M., & Yusef-Zadeh, F. 1993, ApJ, 412, 684

Mendoza C. 1983, in IAU Symposium 103, Planetary Nebulae, ed. R. Flower (Dordrecht: Reidel), 143

Meyer, J.- P. 1989, in AIP Conference Proceedings 183, Cosmic Abundances of Matter, ed. C. J. Waddington, (New York: AIP), 245

Mezger, P. G. & Henderson, A. P. 1967, ApJ, 147, 471

Mezger, P. G., Pankonin, V., Schmid-Burgk, J., Thum, C., & Wink, J. 1979, A&A, 80, L3

Najarro, F., Kudritzki, R. P., Cassinelli, J. P., Stahl, O., & Hillier, D. J. 1996, A&A, 306, 892

Nussbaumer, H. & Storey, 1986, A&A, 64, 545

Osterbrock, D. E. & Flather, E. 1959, ApJ, 120, 26

Pagel, B. E. J. & Patchett, B. E. 1975, MNRAS, 172, 13

Panagia, N. 1973, AJ, 78, 929

Panagia, N. & Walmsley C. M. 1978, A&A, 70, 411

Pardi, M. C., Ferrini, F., & Matteucci, F. 1995, ApJ, 444, 207

Wink, J. E., Altenhoff, W. J., Mezger, P. G. 1982, A&A, 108, 227

Wood, D. O. S. & Churchwell, E. 1989, ApJS, 69, 831

Woodward, C. E., Helfer, H. L., & Pipher, J. L. 1985, A&A, 147, 84

Woosley, S. E., Timmes, R. X., & Weaver, T. A. 1993, J. Phys., G.: Nucl. Part. Phys, 19, S183

Wyse, R. F. G. & Gilmore G. 1995, AJ, 110, 2771

Yusef-Zadeh, F., Zhao, J.- H., & Goss, W. M. 1995, ApJ, 442, 646

Zaritsky, D., Kennicutt, R. C., & Huchra, J. P. 1994, ApJ, 420, 87

This preprint was prepared with the AAS LaTeX macros v4.0.

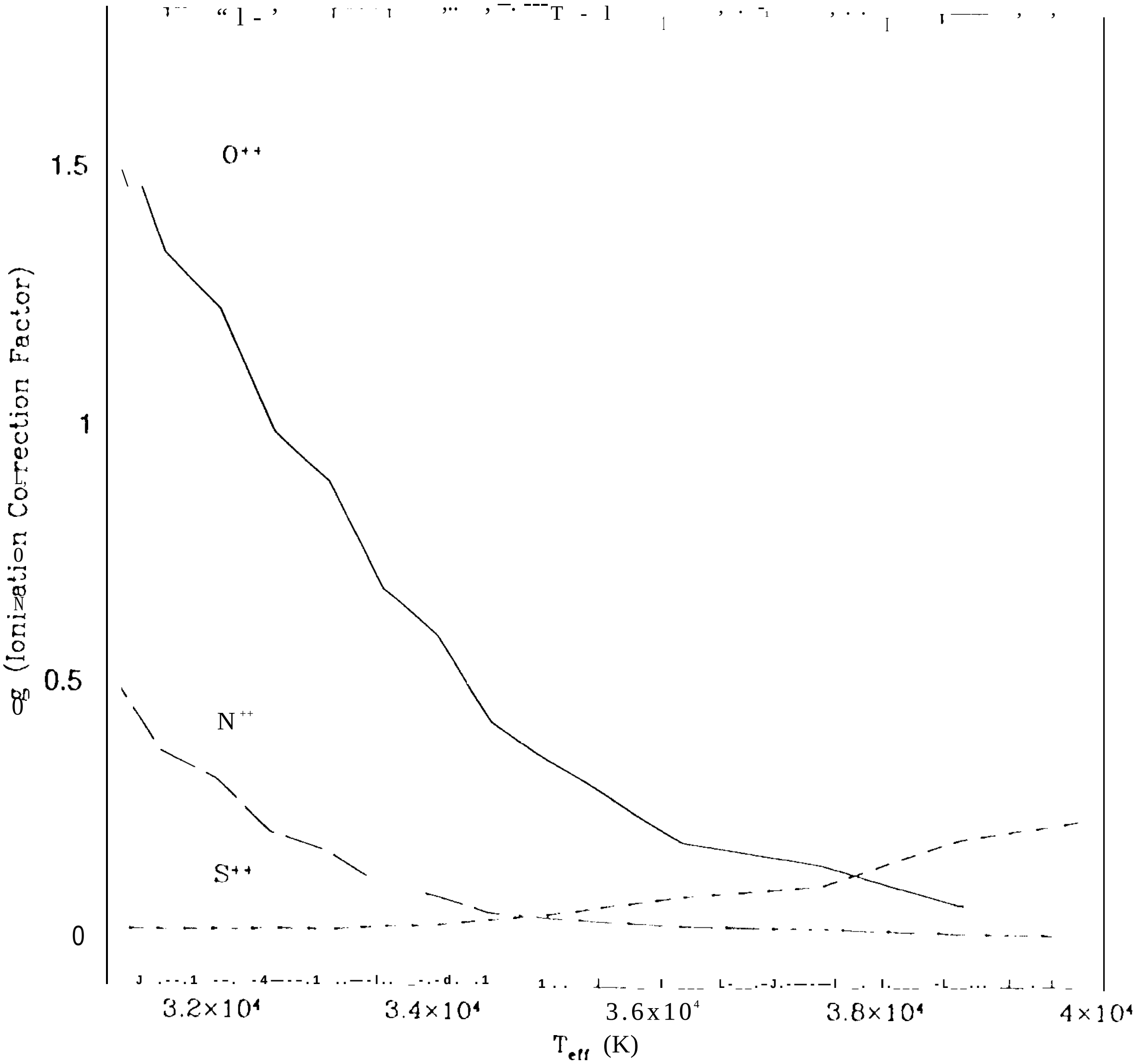

Fig. 2: The ionization correction factor (Z / Z⁺+) is shown as a function of T_{eff} of the ionizing star. The models are for $\log(N_c') = 49$, $f = 0.1$, and n_e = 1000 cm⁻³. 0 / O^{++} changes by up to 0.2 dex between stellar atmosphere models. 'here is a smaller variation in S / S^{++} and h' / N^{++} with T_{eff}.

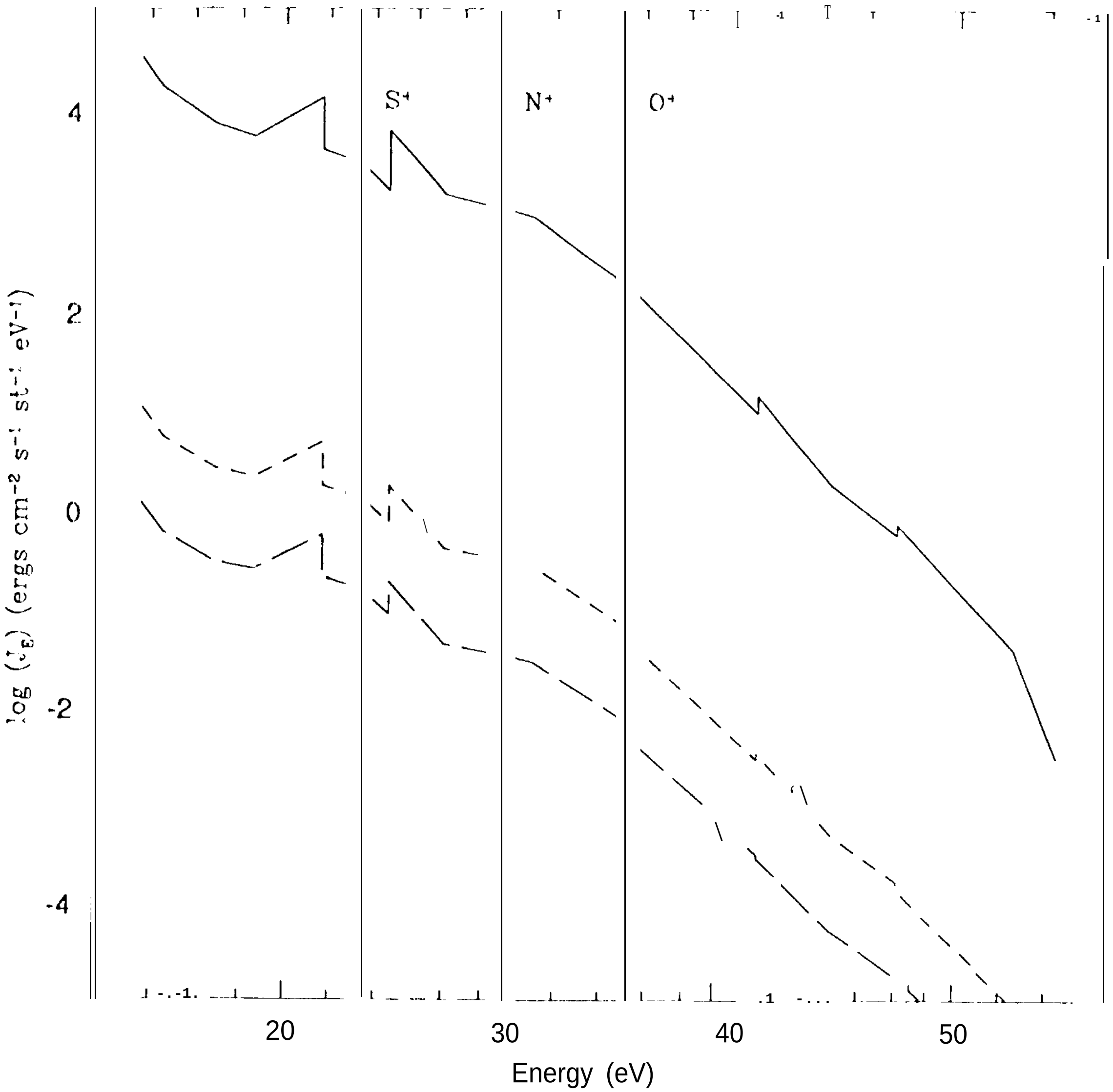

Fig. 4a: The mean intensity of the radiation field is plotted as a function of photon energy at three distances from the central star of G32.80 (T_{eff} = 38750 K). The ionization potentials of S^+, N^+, and O^+ are shown. The solid line is at $r = 5\ 10^{-3}$ PC, the short-dash line is at r = 0.20 PC, just outside the boundary of the core-halo interface, and the long-dash line is at r = 0.6 PC. 'I'he optical depths at 912 Å are 6.6 10^{-6}, 0.73, and 0.87, respectively. The moderate opacities at 912 Å occur only near the boundary of the core and beyond; over most of the core, the opacity is very small.

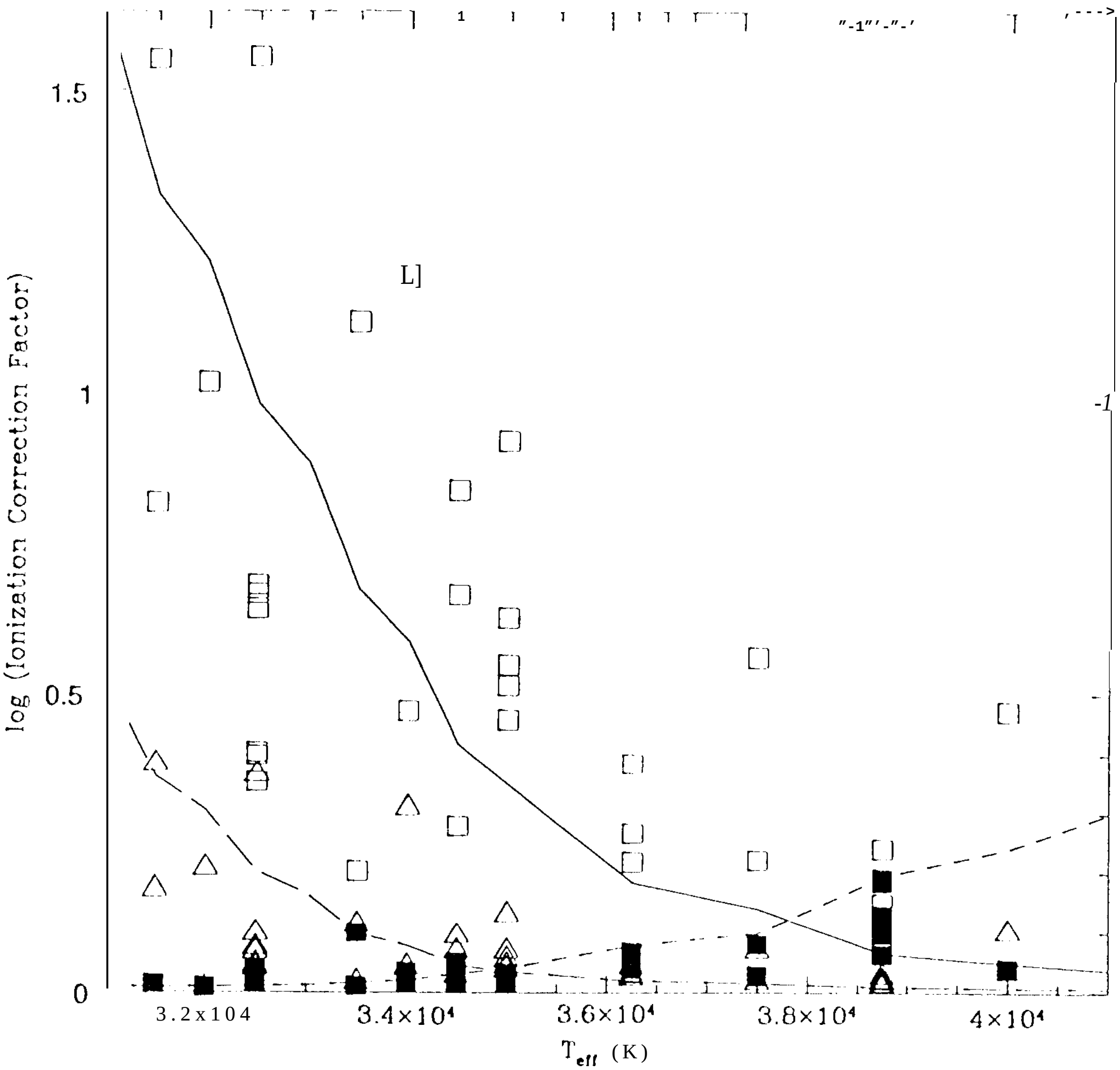

Fig. 5: The ionization correction factors (Z / Z^{++}) of O^{++} (empty squares), N^{++} (empty triangles), and S^{++} (filled squares) are shown as a function of T_{eff}. The observations agree with the theoretical predictions in Figure 2, shown here as solid (O / O^{++}), long-dashed (N / N^{++}), and short-dashed (S / S^{++}) lines. The scatter of the points from the models is due to the range of n_e, AC*, and Z from nebula to nebula.

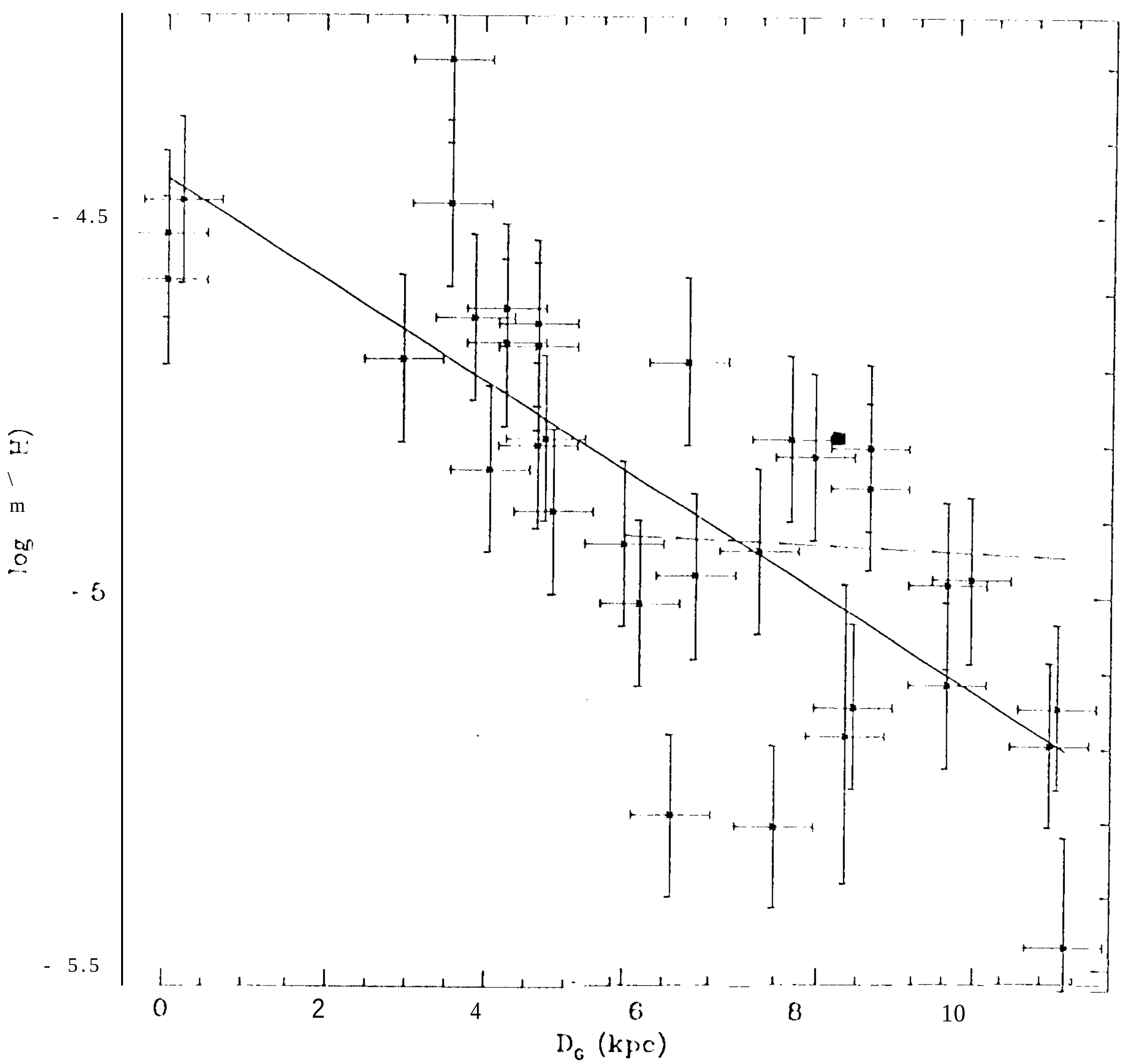

4.5
5
5.5
log m/H
0
2
4
6
8
10
D_G (kpc)

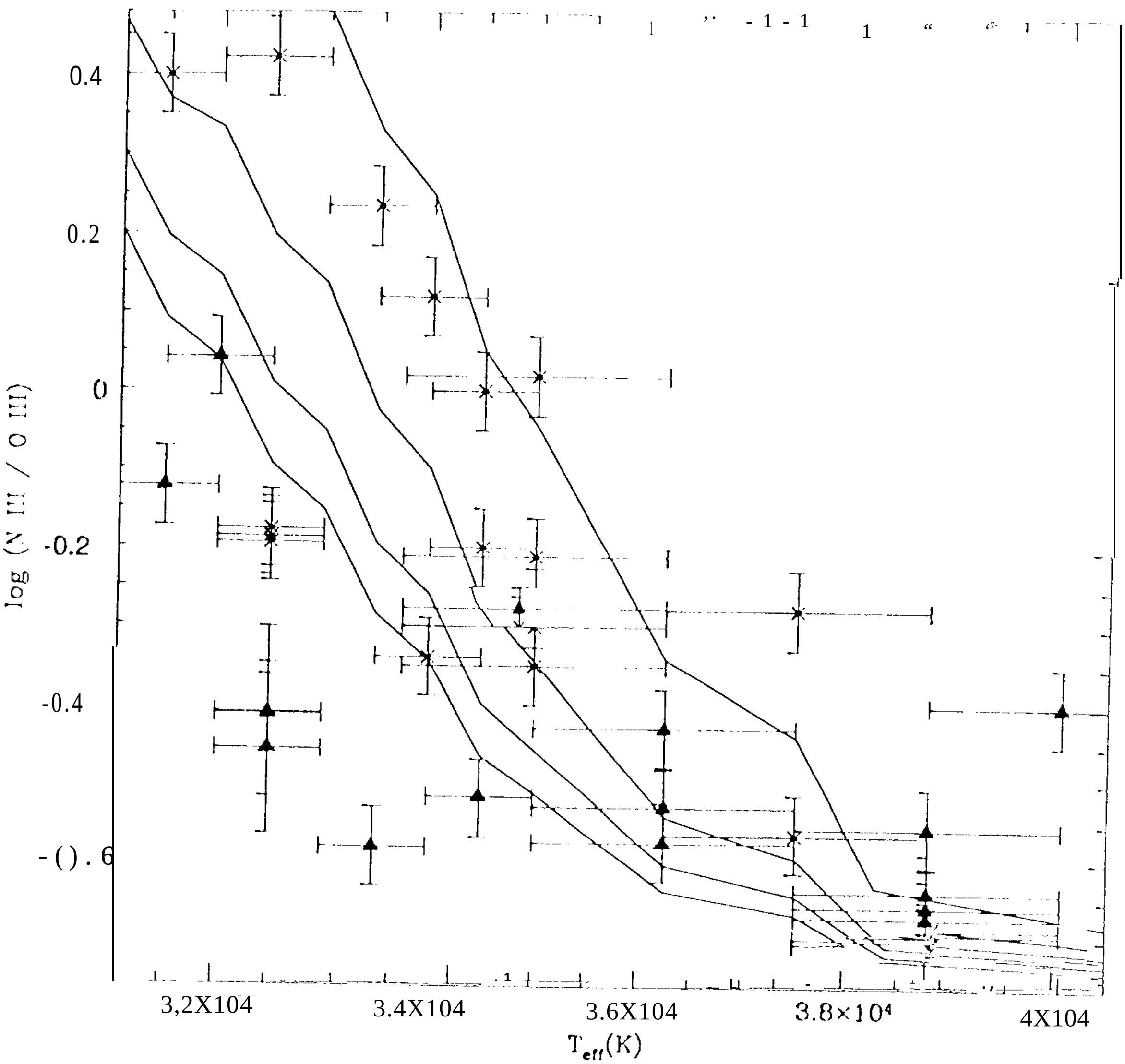

Fig. 9b: Points are the ion ratios as a function of derived T_{eff}. The triangles are sources at $D_G > 6$ kpc; the crosses are sources at $D_G < 6$ kpc. In order of increasing N^{++}/O^{++}, the lines are abundances [Z / H] = -0.4, 0, 0.4, and 0.8 Orion. There is additional scatter in the theoretical ratios of ± 0.06 dex due to the range of n_e and N_c' of our sources. Most sources fall within the range of the models.